https://doi.org/10.5194/egusphere-2026-714
Preprint. Discussion started: 10 March 2026


# Lessons learned from UAV surveys over drifting sea ice at high latitudes

Niklas Neckel[1], Niels Fuchs[2], Jonathan Kolar[3], Thomas Kordes[1], and Christian Haas[1]

[1]Alfred-Wegener-Institut, Helmholtz-Zentrum für Polar- und Meeresforschung, Bremerhaven, Germany
[2]Institute of Oceanography, University of Hamburg, Germany
[3]Institute of Earth Sciences, University of Lausanne, Switzerland

**Correspondence:** Niklas Neckel (niklas.neckel@awi.de)

**Abstract.** In this study, we provide an overview of the challenges encountered when operating consumer grade Unmanned Aerial Vehicles (UAVs) or drones over high-latitude Arctic pack ice. A major obstacle in generating void-free orthomosaics and Digital Elevation Models (DEMs) of ice floes is their drift speed, which can easily exceed 0.5 m $s^{-1}$ in the central Arctic Ocean. Furthermore, there is no commercial solution for operating UAV grid flight missions north of 85° N latitude. To address these issues, we tested and present a novel approach for flying autonomous grid missions at high latitudes including a pre- and post-flight drift correction scheme. Using the resulting data, we generated drift-corrected orthomosaics and DEMs for all ice floes visited during the ArcWatch-2 cruise in August/September 2024. In addition to the UAV camera system we tested a drone based laser scanner and incorporated measurements from drifting Global Navigation Satellite System (GNSS) stations for referencing and validation. Finally, we demonstrate the potential of drone acquired data for deriving ice thickness estimates, surface type classifications and melt pond depth retrievals. Our results offer the potential to upscale in situ measurements and can contribute to better mass balance estimates and meltwater quantification.

## 1 Introduction

In the future, Unmanned Aerial Vehicles (UAVs), or drones, may become a standard tool for sea-ice observations, offering a cost-efficient complement to helicopter-based systems with the capability to operate under weather conditions that might restrict helicopter flights for safety reasons. Furthermore many drones are pollution free, noiseless and easy to handle giving the opportunity to monitor the highly vulnerable polar environment in an adapted and less expensive way. While flying off-the-shelf drones over stable ground at mid latitudes is almost trivial we encountered several problems over high Arctic drift ice for which we found solutions or give suggestions for upcoming expeditions. Problems range from icing and battery lifetime due to low temperatures to issues related to drifting ice floes and the inability to display the drone's position north of 85° N latitude. During the ArcWatch-2 *RV Polarstern* Expedition we had the opportunity to fly two off-the-shelf drone systems, namely a DJI Mavic 3 and a DJI Matrice 350 RTK over drifting sea ice. While the DJI Mavic 3 is a consumer grade camera drone, the DJI Matrice 350 RTK was equipped with a laser scanner to capture the surface topography of the ice. All drone surveys were carried out by authorized pilots in accordance with all applicable legal requirements.

The overarching research goal of the ArcWatch-2 cruise was a multidisciplinary, large-scale assessment of environmental

https://doi.org/10.5194/egusphere-2026-714
Preprint. Discussion started: 10 March 2026


changes in the central Arctic Ocean and on the Barents Sea continental slope (Rabe and Geibert, 2025). Between 2024-08-16 and 2024-09-26 the *RV Polarstern* was moored to 10 larger ice floes across the entire Arctic Ocean (ice stations, Tab. 1) giving the opportunity to test drone operations and to measure relevant sea ice parameters such as ice drift, ice thickness, ice/snow densities and meltpond depths. The acquired drone data were processed to orthomosaics and DEMs for all ice stations building a valuable dataset for all ice related work conducted during the expedition. Initial maps were generated in near-real time, i.e. while the vessel was still moored to the ice floe, supporting in-field decision-making and logistics. Building on this approach, we propose to routinely produce such high-resolution snapshots across different spatial and temporal scales throughout the Arctic Ocean during future cruises.

In-depth analyses of the acquired datasets enabled the derivation of melt pond depth and sea-ice thickness estimates from the DEMs, which were compared with simultaneously acquired *in situ* measurements. This is an important step towards up-scaling *in situ* observations of ice thickness and melt pond depth to the scale of entire ice floes, which is essential for improved mass balance estimates and for the development and parameterization of sea-ice models.

**Table 1.** List of ice stations visited during Arcwatch-2 including average geographic positions for the respective reference date and time.

| Ice station | Date and time | Latitude | Longtitude |
|---|---|---|---|
| PS144_007_01_ICE01 | 2024-08-16 17:00:00 | 85.05805 | 42.93493 |
| PS144_023_01_ICE02 | 2024-08-29 22:00:00 | 84.50036 | 115.72034 |
| PS144_042_01_ICE03 | 2024-09-02 23:00:00 | 84.83094 | 128.87743 |
| PS144_050_01_ICE04 | 2024-09-05 09:09:21 | 85.02579 | 139.94363 |
| PS144_067_01_ICE05 | 2024-09-08 15:00:00 | 84.94667 | 162.09426 |
| PS144_080_01_ICE06 | 2024-09-11 01:00:00 | 84.93331 | 179.41320 |
| PS144_085_01_ICE07 | 2024-09-13 09:00:00 | 87.50035 | 178.72568 |
| PS144_109_01_ICE08 | 2024-09-19 09:20:15 | 89.95154 | -142.69616 |
| PS144_123_02_ICE09 | 2024-09-23 10:00:00 | 88.07016 | 59.95280 |
| PS144_134_01_ICE10 | 2024-09-26 06:00:00 | 87.04715 | 57.07384 |

## 2 Data and Methods

### 2.1 GNSS data

Depending on the duration of the ice station and safety restrictions we were able to install between 3 and 6 autonomous Global Navigation Satellite System (GNSS) stations per ice station serving as Ground Control Points (GCPs) for UAV surveys. These consist of one Novatel FlexPak6 L-Band GNSS receiver, one Novatel choke ring antenna, one data logger and one battery (Neckel et al., 2020). The antennas were mounted on the cases housing the GNSS receiver, data logger and battery. GNSS data were logged every 5 s and were processed employing the Canadian Spatial Reference System Precise Point Positioning (CSRS-PPP) service (Tétreault et al., 2005). The processed GNSS data are referenced to the International Terrestrial Reference

https://doi.org/10.5194/egusphere-2026-714
Preprint. Discussion started: 10 March 2026


Frame 2020 (ITRF2020). Both raw and post-processed GNSS data for all ice stations visited during ArcWatch-2 are available at Neckel et al. (2025b). Next to each GNSS station we drilled through the ice and measured the local ice thickness and freeboard. Additionally, we manually measured the snow thickness and antenna height above the ice surface.

### 2.2 UAV camera flights

#### 2.2.1 Flight preparation

To obtain information on the surface characteristics of each ice station we conducted manual and automatic grid flights employing a DJI Mavic 3 consumer grade drone. The DJI Mavic 3 drone is equipped with a Hasselblad L2D-20C camera including a 4/3 CMOS Sensor. Operating north of 85° N required us to develop our own flight-planning solution for automatic grid flights, as commercial software does not support these extreme latitudes. We further implemented a pre-flight drift correction in the mission planning, which is needed when flying automated grids over drifting sea ice. For our in house flight-planning solution we made use of the waypoint function of the drone which saves manually entered waypoints into KMZ file format. This waypoint file defines which action the drone is executing at a specific geographic position. By employing the QGIS *Flight Planner* plugin and information on the camera's focal length, altitude and sensor size we generated a flight plan at an arbitrary geographic position covering an area of approximately 600 $m^2$. Using a flight speed of 10 m $s^{-1}$, an altitude of 100 m above the ice surface and an image overlap of 80% and 60% along track and across track respectively results in ∼20 minute flight time falling well within the power restrictions of the drone. After generating the shot positions of the camera we run a python application which translates and rotates the grid to a flight path at a given distance parallel to the vessel.

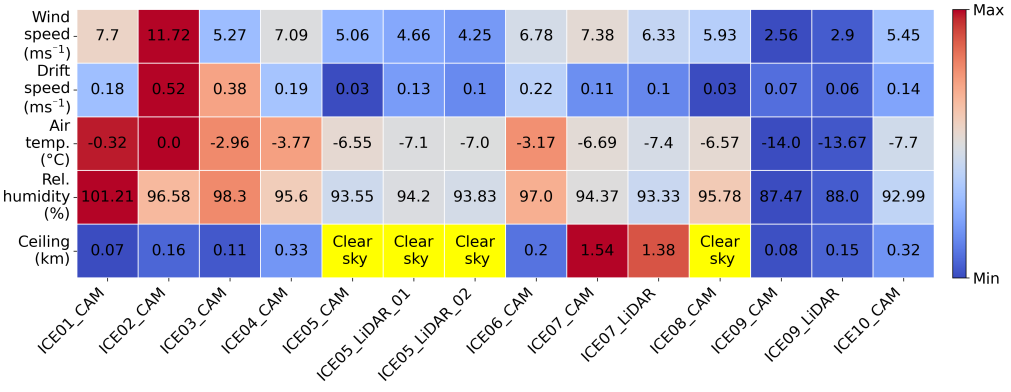


**Figure 1.** Environmental conditions at UAV surveys conducted during the PS144 expedition. Here the average values of the listed parameters in the time of the respective UAV flight are shown. The x-axis is labeled by the ice station number with *CAM* for an UAV camera flight or *LiDAR* for an UAV LiDAR survey. The reference times of all ice stations are listed in Table 1. Colors are normalized to min-max of the respective variable.

https://doi.org/10.5194/egusphere-2026-714
Preprint. Discussion started: 10 March 2026


Depending on the wind and ocean currents sea ice is constantly drifting. During the ice stations of PS144 we found high drift speeds between 0.03 and 0.52 m $s^{-1}$ (Fig. 1). To account for this it is mandatory to correct the estimated flight path for the ice drift during the survey. Otherwise a sufficient image overlap of the same ice can not be guaranteed resulting in data gaps in the final orthomosaics. Under the assumption that the ice drift remains constant during the flight, we corrected the single camera positions with drift vectors calculated from 10 minute logs of a handheld GPS device just prior to the flight resulting in a pseudo Lagrangian grid mission (Fig. 2a). When the vessel was moored to an ice floe also the course and speed of the vessel could be employed as a drift estimate saving some time in the mission preparation. Based on the estimated ice drift we also included an arbitrary time delay which gives the drone pilot the necessary amount of time to upload the flight-plan to the drone and move to a safe launch site, such as the helicopter pad or the ice floe the vessel is moored to. The adjusted waypoints are finally saved in the initial KMZ format, replacing the original file on the controller. The entire workflow is wrapped in a Python environment and is publicly available via GitLab. Before takeoff the operator needs to manually adjust aperture, shutter speed and iso value of the camera to the prevailing lighting conditions and ice surface characteristics. This holds true for both manual and automatic grid flights. For the UAV camera data obtained during the ArcWatch-2 cruise we used a fixed aperture of f/2.8, iso values between 100 and 400 and shutter speed timings between 1/640 and 1/1600 s. All images are stored in DNG and JPG format on the memory card of the drone.

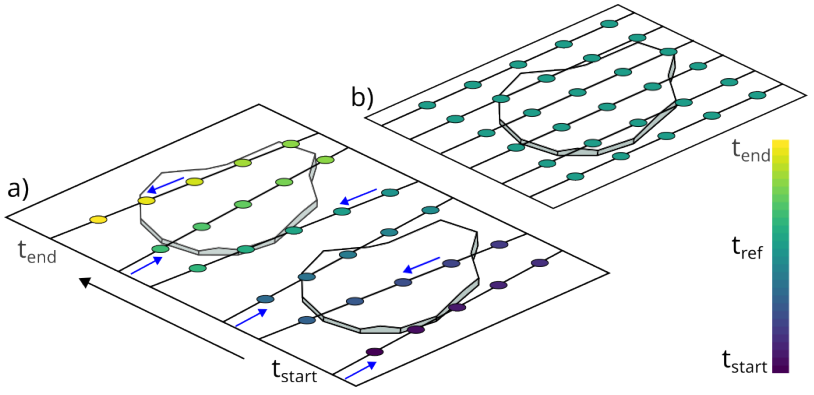


**Figure 2.** Scheme of pre- and post-flight drift correction of UAV camera grid flights. The ice drift (black arrow) is measured prior to the flight and is included in the mission planing resulting in a pseudo Lagrangian grid mission (**a**), time is indicated by color gradient and flight direction of the UAV by blue arrows). In the post-processing GNSS drift estimates are used to transfer the image locations into an Eulerian coordinate system using a fixed reference time **b**).

s

### 2.2.2 Generation of Orthomosaics and Digital Elevation Models

Orthomosaics and DEMs were generated for all ice stations listed in Table 1. After an initial quality check we used the images stored in JPG format on the memory card of the drone. Independent if the data were acquired manually or via our automatic grid flight routine all images were drift corrected to the reference time stamps listed in Table 1 (Fig. 2b). For this we extracted the

https://doi.org/10.5194/egusphere-2026-714
Preprint. Discussion started: 10 March 2026


time and camera position from the exif metadata of each image. We then selected one GNSS reference station and calculated the difference in meters between the position of the respective reference GNSS station at the reference time shown in Table 1 and at the acquisition time of each image. For the latter the GNSS data were interpolated to the exact acquisition time of the respective image. This estimate was used as an initial drift correction and has been proven mandatory elsewhere (Hyun et al., 2019; Neckel et al., 2023; Steer and Divine, 2024).

The images including information on their drift corrected locations and attitude angles were imported into the commercial Agisoft Metashape software (Agisoft LLC, 2021). Additionally, the GNSS solutions from our drifting reference stations at the reference times listed in Table 1 were imported into the software and were used as GCPs during the processing (the total number of GCPs per ice station is listed in Tab. 2). After the generation of tie points from the drift corrected images the choke ring antennas were selected in a couple of images and assigned to the nearest GCP. Then a camera optimization step was performed to improve the camera positions now aided by the more precise GNSS reference solutions. In order to test the influence of GCPs on the accuracy of the final DEMs we included 1) no GCPs, 2) 3 GCPs forming the largest triangle possible and 3) all GCPs in the photogrammetric processing (Tab. 2). In the next step a dense point cloud was generated which was gridded to an individual DEM for each ice floe. If an overall elevation trend was observed in the derived DEM we applied an additional fit to the data to adjust with sea level. Depending on the shape of the elevation trend, we subtracted either a linear or a quadratic fitted surface from the DEM. In a last step the single images were projected on the respective DEM and stitched to a final orthomosaic for each ice station.

#### 2.2.3 Sea-ice surface properties retrieved from camera data

The implementation of drones aims to facilitate and expand studies of the ice surface and related processes. Therefore, we tested new algorithms recently developed for helicopter-borne systems using drone-acquired data. This includes an automatic pond detection with the classification algorithm PASTA-ice (Fuchs, 2023) and a melt pond depth retrieval (Fuchs et al., 2024). Due to the abundance of open melt ponds, we selected flight *ICE01_CAM* as a test case (Tab. 1 & Fig. 1). Classification of the RGB orthomosaic (Fig. 3a) with PASTA-ice yields maps with every pixel assigned to a surface-type class, allowing for the derivation of areal melt pond fractions (e.g., 27% at ICE01) and vector polygons that encompass all adjacent pixels of similar types, such as a single melt pond. Using these polygons, we then determine the height of pond margins in the photogrammetrically derived DEM (Fig. 3b), thus retrieving the pond level above sea level. With the correction for refraction at the air-pond interface, introduced in Fuchs et al. (2024), we derive pond depth in a two-media photogrammetry approach (Fig. 3).

### 2.3 UAV Lidar flights

#### 2.3.1 Flight preparation

For flying the DJI Matrice 350 RTK drone with the Zenmuse L2 LiDAR module we needed to operate a DJI D-RTK 2 mobile base station on the aft corner of the helicopter pad from where also the UAV was launched manually. Before the actual scanning, an automatic calibration pattern was carried out by the flight system. The measurement itself consisted of a long straight line

https://doi.org/10.5194/egusphere-2026-714
Preprint. Discussion started: 10 March 2026


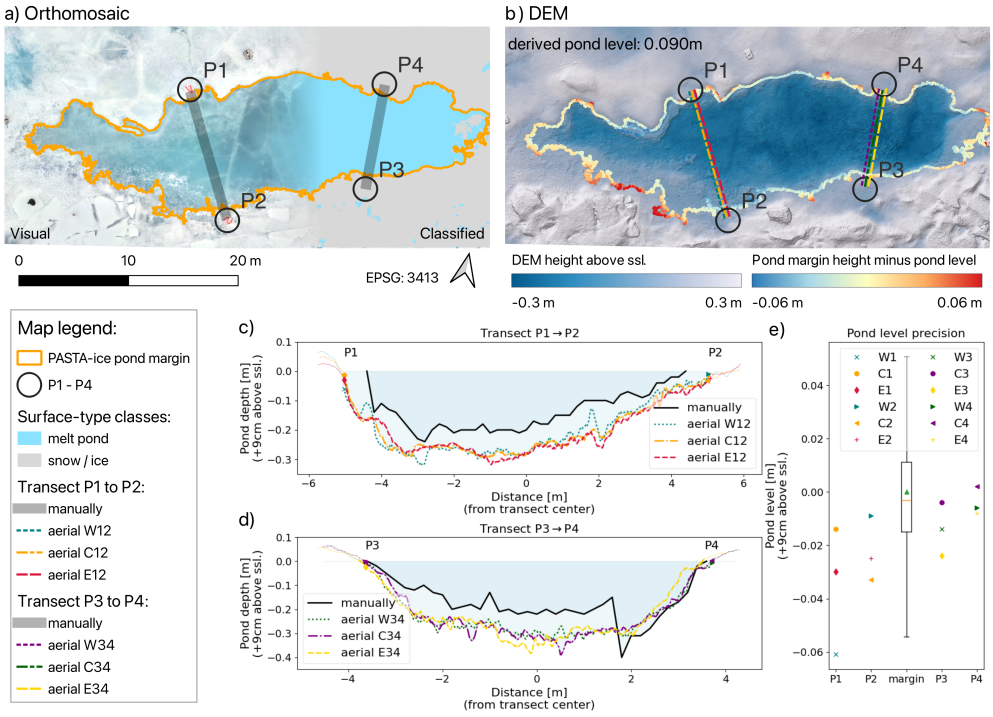


**Figure 3.** Sea-ice surface properties derived from UAV flight ICE01_CAM. Map of the ice surface around the main studied pond **a)**, showing the brightness corrected RGB orthomosaic on the left and the classification into main surface-type classes (grey: snow/ice, blue: ponds) on the right overlaid on the DEM. Example of pond depth retrieval including its vertical derivation from the mean pond level (**b**). Manual pond depth measurements along the two profile lines marked in **a)** and derived from the UAV data along three parallel lines at these locations (W, C, and E) are provided in panels **c)** and **d)** with water-filled area shaded in blue. Panel **e)** shows the estimated pond level at the transect pond edges from the mean pond level (markers) and along the entire pond margin (box and whiskers plot).

at a constant flight altitude between 100 m and 200 m. At the end of the survey, the system performed another automatic calibration pattern.

### 2.3.2 Generation of Digital Elevation Models

When employing DJI's L2 LiDAR module the user is forced to use DJI's Terra software for reading the acquired data. Also data from a nearby DJI D-RTK 2 mobile base station needs to be available for the time period of data acquisition and imported into the software. LiDAR data were successfully acquired at ice stations ICE05, ICE07 and ICE09 and exported in common LAS point cloud format from DJI's Terra software. We then applied a similar drift correction scheme as for the UAV camera data on the georeferenced point cloud data to match the reference date and time shown in Table 1. The drift corrected point clouds were imported into the open CloudCompare software and referenced to the available GNSS derived GCPs. For ice station ICE05 data from two LiDAR flights were available (Fig. 1) and their point clouds were merged after referencing them

https://doi.org/10.5194/egusphere-2026-714
Preprint. Discussion started: 10 March 2026


to the available GCPs (Figs. 4c and d). Finally all point clouds were gridded to a spatial resolution of 0.15 m, resulting in a DEM for ice stations ICE05, ICE07 and ICE09. Similar to the photogrammetric DEMs we removed slight elevation trends by subtracting either a linear or a quadratic fitted surface from the DEMs.

### 2.4 Ice and snow thickness retrievals

During Arcwatch-2 ice thickness was measured directly by drilling and by sled based multi-frequency electromagnetic induction measurements (GEM-2, Geophex Ltd.) for all ice stations. While drill measurements result in the actual ice and snow thicknesses at a specific location, the GEM-2 measures the distance from the snow surface to the ice–ocean interface resulting in a total ice+snow thickness estimate (Itkin et al., 2023; Neudert et al., 2024). To retrieve the actual ice thickness, additional snow depth measurements were carried out along the GEM-2 transects employing a Magnaprobe device (Itkin et al., 2023). Both the GEM-2 and the Magnaprobe device record GNSS positions and timestamps which were used for a similar drift correction as for the drone data to match the reference date and time shown in Table 1. In the next step both datasets were resampled onto a common, equidistant track at 1.5 m point spacing so that each point contains both snow and ice-thickness information (Kolar et al., 2025). Importantly, all GEM/Magnaprobe transects were conducted prior to the UAV flights. The clearly visible footpaths in the corresponding orthomosaics allowed for additional horizontal corrections by aligning the equidistant track files to these features.

As a case study we converted both the photogrammetric and the LiDAR DEMs of ice station ICE05 into ice thickness estimates assuming hydrostatic equilibrium. For this we converted the ellipsoidal DEM elevations into freeboard estimates employing the *in situ* freeboard measurements conducted at each GNSS station. Furthermore we used average snow depth measurements of the conducted magnaprobe survey, *in situ* measurements of ice and snow densities and a fixed density of 1023.9 kg $m^{-3}$ for sea water to calculate ice thickness from freeboard.

## 3 Results

Photogrammetric DEMs and orthomosaics were derived for all 10 ice stations of the PS144 expedition and are available at Neckel et al. (2025a). Table 2 summarizes the vertical DEM accuracy ($1\sigma$) when compared to the available local GNSS measurements. Final DEMs include all GCPs in the processing and were adjusted with an additional vertical fit to adjust with sea level if required. The poorest vertical accuracies of 0.23 and 0.21 m were found for ICE07 and ICE09, respectively, with both ice stations characterized by low visibility and low ground contrast (Fig. 1 & Tab. 1). Under favorable conditions, vertical accuracies as good as 0.03 m were achieved (Tab. 2). Based on the photogrammetric DEMs we show results on melt pond depth retrievals for ice station ICE01, i.e. the only ice station with open melt ponds visited during the ArcWatch-2 expedition (Tab. 1 & Fig. 3). Comparing aerial with manually measured pond depths along two transect lines (P1-P2 and P3-P4) (Fig. 3c and d), reveals a highly variable pond bottom and a general overestimation of pond depth from the aerial approach by 6 cm on average. Due to the imprecise co-location of the transect, we extracted three closely spaced parallel lines (W, C, and E) from the aerial data. Most local features of the manual observations, except for a trench close to P4, are visible in at least one of

https://doi.org/10.5194/egusphere-2026-714
Preprint. Discussion started: 10 March 2026


these lines, highlighting the generally efficient retrieval. Inaccuracies in the reconstructed DEM and pond margin classification probably caused an overestimation of the pond level of up to 6 cm close to the transect points (Fig. 3e), contributing to the overall depth overestimation.

We further show the potential of photogrammetric and LiDAR DEMs for the derivation of freeboard and ice thickness assuming hydrostatic equilibrium (Fig. 4). Over flat ice areas where this assumption holds true, our results agree well with *in situ* drill and EM measurements. This is evident from Figure 4e where all measurements show average ice thicknesses between 1.2 and 1.3 m. Overall we found that UAV borne LiDAR has great potential and robust results could be obtained also in conditions were photogrammetric retrievals fail. When comparing the UAV LiDAR DEMs to the local GNSS reference measurements we obtain vertical accuracies between 0.02 and 0.15 m.

**Table 2.** Validation of GCP distribution on the UAV derived DEMs. Each ice station includes between 3 and 6 GCPs for referencing and validation. Here we show the average deviation to all GCPs with *No GCPs*, *3 GCPs*, *All GCPs* and if required with an *Extra fit* included in the photogrammetric processing. Also the vertical accuracy ($\pm 1\sigma$) is shown for all estimates.

| Station | No GCPs | 3 GCPs | All GCPs (#) | Extra fit |
|---|---|---|---|---|
| ICE01* | 16.98±0.16m | 0.09±0.09m | 0.09±0.07m (4) | - |
| ICE02* | 6.06±0.15m | 0.1±0.11m | 0.02±0.03m (6) | - |
| ICE03*† | 8.31±0.71m | 0.13±0.14m | - (3) | 0±0.03m |
| ICE04† | -14.74±1.01m | -1.26±1.36m | 0.04±0.08m (6) | 0±0.07m |
| ICE05† | -0.85±0.48m | 0.03±0.12m | 0.01±0.12m (6) | 0±0.03m |
| ICE06† | 8.56±0.74m | 0.58±0.81m | 0.07±0.14m (4) | 0±0.05m |
| ICE07† | 21.57±1.08m | 1.52±1.22m | 0.35±0.23m (6) | - |
| ICE08* | 4.13±0.12m | 0.04±0.11m | 0.16±0.14m (5) | 0±0.04m |
| ICE09† | 16.39±0.53m | 0.01±0.23m | 0.04±0.21m (4) | - |
| ICE10† | 20.88±2.06m | 0.52±0.55m | 0.13±0.04m (5) | - |

* Manual flight, † Grid flight, # Number of GCPs

## 4 Discussion and Conclusion

Comparing the results from different ice stations remains difficult as different environmental conditions were prevailing and different flight patterns were conducted. However, in the following we draw some conclusions from the results obtained from the drone flights conducted during the PS144 expedition.

Flying drones in Arctic conditions comes with several challenges for both the UAV and the pilot. For example, under foggy conditions propeller icing can be a serious issue, potentially leading to electric-motor overheating, and thus de-icing measures may be considered (Hann et al., 2021). Furthermore, the tested drones and commercial software packages for automated grid-flight planning do not support the display of positions >85° N latitude. In particular, the pilot cannot follow or plan the drone path on a map display, highlighting the need for the approach introduced in this study.

https://doi.org/10.5194/egusphere-2026-714
Preprint. Discussion started: 10 March 2026


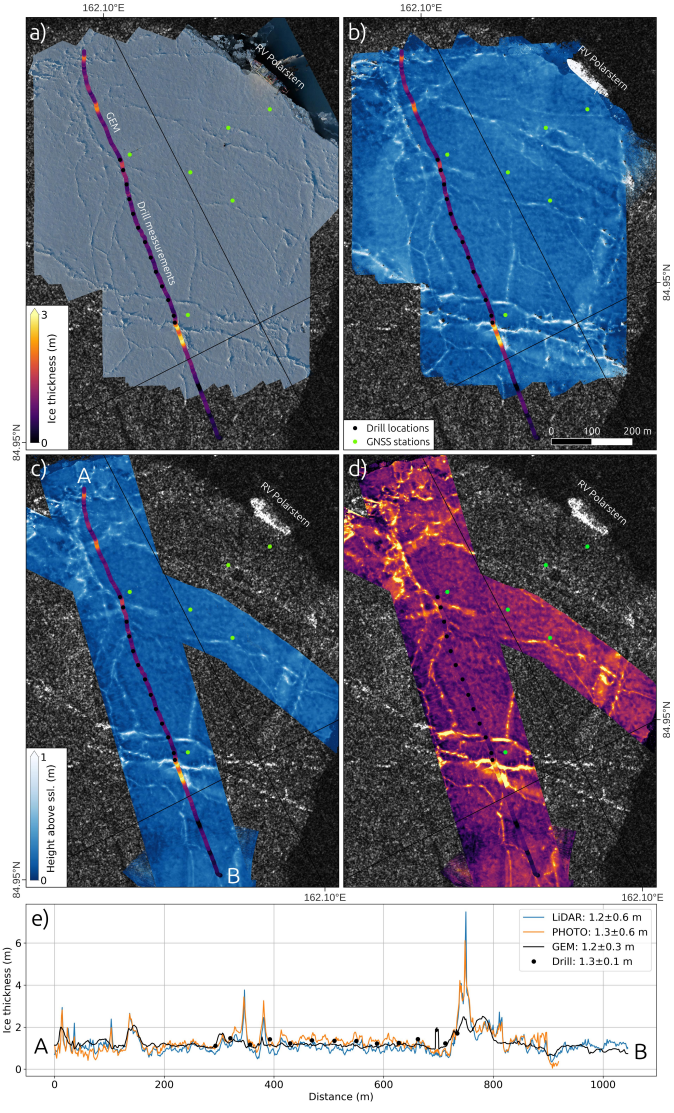


**Figure 4.** Results of UAV flights on 2024-09-08 (ICE05). Clear sky conditions and low ice drift (0.03 – 0.13 m $s^{-1}$) made this ice station ideal for drone operations. Orthomosaic and photogrammetric DEM are shown in panel **a)** and **b)** respectivley. LIDAR drone flights 5.1 and 5.2 are shown in panel **c)** while panel **d)** shows the inferred ice thickness estimates from the LiDAR flights. All maps are superimposed on a COSMO-SkyMed SAR image acquired on 2024-09-08 at 07:38:14 UTC and translated to the reference time shown in Table 1 (COSMO-SkyMed Product - ©ASI - Agenzia Spaziale Italiana - 2024). Ice thickness estimates are shown along the GEM profile A – B in panel **e)**.

The conducted UAV camera flights can be separated into manual flights and grid flights, with the latter incorporating a priori drift information into the flight planning (Fig. 2). UAV grid flights can cover large areas being highly efficient in terms of flight time and hence power supply of the drone. Even under poor environmental conditions data from grid flights can be used for stitching orthomosaics making it an ideal tool for quickly generating orthorectified maps of large ice floes. Here we find

https://doi.org/10.5194/egusphere-2026-714
Preprint. Discussion started: 10 March 2026


that both a pre and post flight drift correction is mandatory to obtain void-free results. Furthermore, redundant overpasses are minimized, and the drone pilot is spared the discomfort of cold hands - another serious issue when operating drones in polar environments. However, when detailed terrain reconstructions are needed for e.g. melt pond depth retrievals or ice thickness/freeboard estimates images from multiple look angles are required. This becomes evident from Table 2 where we found a higher vertical accuracy ($1\sigma$) when using no GCPs from manual flights than from grid flights. Therefore we found results from manual flights more sophisticated for tasks requiring high accuracies but grid flights could be adapted in the future to also fulfill these requirements employing more complex flight patterns such as drift corrected cross-grid and additional oblique image flights (Elias et al., 2024).

During the UAV camera flights at ice stations ICE07 and ICE09 we encountered poor to bad visibility with very little contrast on the ice/snow surface (Fig. 1). Therefore insufficient tie points were found in a number of images resulting in DEMs of low quality (Tab. 2). However, despite the foggy conditions the L2 LiDAR module performed reasonably well at both ice stations showing the great potential of an active LiDAR system when terrain reconstruction by means of passive photogrammetry fails. Also the wavelength of 905 nm is perfectly suited for snow and ice applications. However, the L2 LiDAR module is not the best system for drifting sea ice conditions as it requires a nearby base station which fails for ice drifts faster $\sim$0.15 m $s^{-1}$. Furthermore the commercial DJI Terra software is needed for processing the raw LiDAR data, leaving no user interaction for ice drift corrections at this stage.

As a case study, we applied recently developed tools to derive sea-ice surface properties from image data. Comparing it to *in situ* measurements of pond depths, we notice an overestimation by 6 cm in the aerial pond depth determination, especially in the absolute depth, while the general gradients are correctly reconstructed (Fig. 3). The deviation exceeds previous evaluations that lacked data from late-season melt ponds (Fuchs et al., 2024). We assume that the ice at the pond bottom of the here observed melt pond has potentially lost scatterers, such as air inclusions through an increased permeability, and thus becomes more translucent, causing a reconstruction of the sub-pond bottom layer. Based on these observations, we recommend further comparisons of the same ponds over the entire melt season, including an analysis of the actual reconstructed layer. Another small part could be attributed to an imprecise pond level determination, either because of steeper pond walls late in the season (Fetterer and Untersteiner, 1998) or horizontal inaccuracies in the determination of where the ice is water-covered in the high-resolution image data. Also, the co-location of the *in situ* measurements seems to be imprecise and could be improved by the use of a tachymeter in the future. Future UAV deployments on campaigns will allow us to gain a better understanding of the error dependencies on pond evolution and morphology, and the technology used.

*Code availability.* The python code for generating drift corrected UAV survey grids is available at https://gitlab.awi.de/nneckel/MAVIC3GRID.

https://doi.org/10.5194/egusphere-2026-714
Preprint. Discussion started: 10 March 2026


*Data availability.* The derived GNSS data are available at https://doi.pangaea.de/10.1594/PANGAEA.983769. The final orthomosaics and DEMs are available at https://doi.org/10.1594/PANGAEA.984115. The ice thickness data for all ice stations are available at https://doi.org/10.1594/PANGAEA.984304.

*Author contributions.* Niklas Neckel developed and tested the drift-correction scheme and wrote the initial manuscript draft. Niels Fuchs contributed to the calculation of pond depth and wrote the corresponding section. Jonathan Kolar contributed to the fieldwork and assisted with processing the GEM-2 data. Thomas Kordes contributed the three LiDAR flights. Christian Haas supervised the study and contributed to writing and editing the manuscript.

*Competing interests.* The authors declare no competing interests

*Acknowledgements.* We thank Benjamin Rabe, Walter Geibert, Janna Rückert, Jonathan Bahlmann, Linnea Bühler, Nils Risse and the entire crew of the PS144 expedition for their help in the field. We further thank Thomas Krumpen for his support from back home and Angelika Humbert for providing 6 GNSS stations.

https://doi.org/10.5194/egusphere-2026-714
Preprint. Discussion started: 10 March 2026


## References

Agisoft LLC (2021). Agisoft Metashape User Manual Professional Edition, Version 1.7.

Elias, M., Isfort, S., Eltner, A., and Maas, H.-G. (2024). UAS Photogrammetry for Precise Digital Elevation Models of Complex Topography: A Strategy Guide. *ISPRS Annals of the Photogrammetry, Remote Sensing and Spatial Information Sciences*, X-2-2024:57–64.

Fetterer, F. and Untersteiner, N. (1998). Observations of melt ponds on Arctic sea ice. *Journal of Geophysical Research: Oceans*, 103(C11):24821–24835.

Fuchs, N. (2023). A multidimensional analysis of sea ice melt pond properties from aerial images.

Fuchs, N., von Albedyll, L., Birnbaum, G., Linhardt, F., Oppelt, N., and Haas, C. (2024). Sea ice melt pond bathymetry reconstructed from aerial photographs using photogrammetry: a new method applied to MOSAiC data. *The Cryosphere*, 18(7):2991–3015.

Hann, R., Enache, A., Nielsen, M. C., Stovner, B. N., van Beeck, J., Johansen, T. A., and Borup, K. T. (2021). Experimental Heat Loads for Electrothermal Anti-Icing and De-Icing on UAVs. *Aerospace*, 8(3).

Hyun, C.-U., Kim, J.-H., Han, H., and Kim, H.-c. (2019). Mosaicking Opportunistically Acquired Very High-Resolution Helicopter-Borne Images over Drifting Sea Ice Using COTS Sensors. *Sensors*, 19(5).

Itkin, P., Hendricks, S., Webster, M., von Albedyll, L., Arndt, S., Divine, D., Jaggi, M., Oggier, M., Raphael, I., Ricker, R., Rohde, J., Schneebeli, M., and Liston, G. E. (2023). Sea ice and snow characteristics from year-long transects at the MOSAiC Central Observatory. *Elementa: Science of the Anthropocene*, 11(1):00048.

Kolar, J., Neckel, N., Rückert, J. E., Bühler, L., Bahlmann, J., Risse, N., Hendricks, S., and Neudert, M. (2025). Ice and snow thickness measurements from the ArcWatch-2 Expedition.

Neckel, N., Fuchs, N., Birnbaum, G., Hutter, N., Jutila, A., Buth, L., von Albedyll, L., Ricker, R., and Haas, C. (2023). Helicopter-borne RGB orthomosaics and photogrammetric digital elevation models from the MOSAiC Expedition. *Scientific Data*, 10(1):426.

Neckel, N., Fuchs, N., Kolar, J., Kordes, T., and Haas, C. (2025a). UAV based orthomosaics and ice surface models from the ArcWatch-2 Expedition.

Neckel, N., Kolar, J., Bühler, L., Bahlmann, J., Rückert, J. E., Trace-Kleeberg, S., and Risse, N. (2025b). GNSS measurements of PS144 ice stations.

Neckel, N., Zeising, O., Steinhage, D., Helm, V., and Humbert, A. (2020). Seasonal Observations at 79°N Glacier (Greenland) From Remote Sensing and in situ Measurements. *Frontiers in Earth Science*, 8.

Neudert, M., Arndt, S., Hendricks, S., Hoppmann, M., Schulze, M., and Haas, C. (2024). Improved sub-ice platelet layer mapping with multi-frequency EM induction sounding. *Journal of Applied Geophysics*, 230:105540.

Rabe, B. and Geibert, W. (2025). The Expedition PS144 of the Research Vessel POLARSTERN to the Arctic Ocean in 2024.

Steer, A. and Divine, D. (2024). Sea ice stations orthophotos and digital elevation models from drone -based aerial surveys conducted during Nansen Legacy cruises to the northern Barents Sea and the area north of Svalbard in 2021-2022.

Tétreault, P., Kouba, J., Héroux, P., and Legree, P. (2005). CSRS-PPP: An internet service for GPS user access to the Canadian Spatial Reference frame. *Geomatica*, 59:17–28.